


Controllable photonic spin Hall effect induced by an off-axis polarization singularityXiang Zhang ¹, Yanke Li,¹ Yuan Zhang,¹ Bingyan Wei ¹, Sheng Liu ¹, Yi Zhang,¹ Peng Li ^{1,2,*} and Jianlin Zhao ^{1,2,†}¹*Key Laboratory of Light Field Manipulation and Information Acquisition, Ministry of Industry and Information Technology, Shaanxi Key Laboratory of Optical Information Technology, School of Physical Science and Technology,**Northwestern Polytechnical University, Xi'an 710129, China*²*Collaborative Innovation Center of Light Manipulation and Applications, Shandong Normal University, Jinan 250358, China*

(Received 1 April 2024; accepted 24 June 2024; published 17 July 2024)

The photonic spin Hall effect (PSHE) with high efficiency is of significance for the application of spin photonic devices, but the spin-dependent separation induced by the refraction or reflection at the interface of the media is too tiny to be used in practice. In this paper, we realize a PSHE by designing off-axis polarization singularity in free space and reveal the relationship between controllable spin-orbit coupling and orbital angular momentum (OAM) spectra of the off-axis vector beam. The numerical simulations and experimental results show that the spin-dependent separated distance and the OAM spectra are manipulated by the embedded position and polarization order of polarization singularity, and the separating direction perpendicular to the off-axis direction of polarization singularity. Our work provides a feasible and simple path for manipulating spin photons toward information processing based on optical spintronics.

DOI: [10.1103/PhysRevA.110.013511](https://doi.org/10.1103/PhysRevA.110.013511)**I. INTRODUCTION**

The photonic spin Hall effect (PSHE) [1,2] has attracted intense research interest for its potential applications in precision metrology [3,4], optical manipulations [5,6], analog optical computing [7,8], etc. This analogy of the spin Hall effect in the electronic system [9] presents the spatial separation of two spin states of light. It is generally an external manifestation of spin-orbit interaction (SOI) [10], which originates from the optical angular momentum [11] and two kinds of geometric phases, i.e., the Rytov-Vladimirskii-Berry (RVB) phase [12,13] and the Pancharatnam-Berry (PB) phase [14]. The former is related to the changing of beam propagation directions, such as the refraction or reflection at the interface of the media; the spin-dependent separation is too tiny to be observed unless weak measurement technology is used [15], but the latter, which is associated with polarization transformation, could significantly enhance the SOI of light [16–19]. Currently, researchers have demonstrated the phenomena of PSHE by exploiting the uniaxial-crystal plates [20,21], photonic graphene [22], surface plasmon nanostructures [23], metasurfaces [24], on-chip devices [25], and so on.

Cylindrical vector beams [26,27] embedded with polarization singularity are classic beams with spatially inhomogeneous polarization, which have been widely used in microfabrication [28,29], optical tweezers [30], high-resolution imaging [31], optical data storage [32,33], and so on. The phenomena of spin-dependent splitting have been unveiled by breaking the rotational symmetry of a cylindrical vector beam. For example, when the incident beam is shifted from the central optical axis of the metasurface [34], using

the fan-shaped baffles [35] induces the discontinuous vortex phases of two spin components in the azimuthal direction, which results in spin accumulation at the opposite edge, or generating large PSHE at near-normal incidence with the metamaterial slab [36], the optical bound states in the continuum (BICS) hosting metasurface [37], the effective q plates in Fourier or real spaces [38], the anisotropic uniaxial crystal [39], and so on. Could the breaking of rotational symmetry induced by off-axis polarization singularity cause the PSHE?

In this paper, we numerically and experimentally investigate the PSHE induced by the off-axis polarization singularity. The influences on PSHE at the focal plane are represented by changing the off-axial distances, the embedded positions, and the polarization order of polarization singularities at the initial plane. Furthermore, the connection between the modulated OAM spectrum and PSHE was discussed. The mechanism of PSHE induced by the off-axis polarization singularity we presented is promising in the unique application of manipulating spin photons, and the universal underlying mechanism of large PSHE in the platforms using a nonperfect vortex.

II. THEORY

In paraxial conditions, the Gauss beam embedded with off-axis polarization singularity [40] could be expressed as the superposition of left- (LCP) and right-handed circularly polarized (RCP) components with off-axis opposite vortex phases; this initial beam in the Cartesian coordinates (x_{in}, y_{in}) can be written as

$$\mathbf{E}(x_{in}, y_{in}) = E_0 \exp\left(-\frac{x_{in}^2 + y_{in}^2}{w_0^2}\right) \times \{\exp[-im(\theta + \theta_0)]\mathbf{e}_L + \exp[im(\theta + \theta_0)]\mathbf{e}_R\}, \quad (1)$$

*Contact author: pengli@nwpu.edu.cn

†Contact author: jlzhao@nwpu.edu.cn

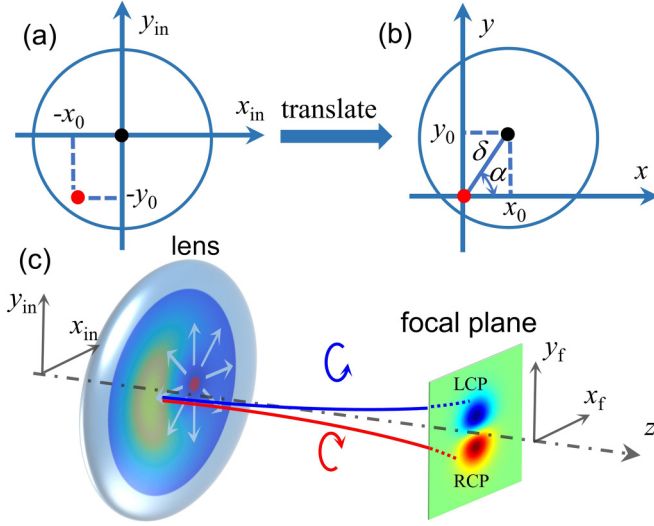


FIG. 1. Gauss beam embedded with an off-axis polarization singularity. (a), (b) Embedded positions of polarization singularity (the red and black dots represent the center of polarization singularity and the Gauss beam, respectively; the blue circle depicts the waist radius). (c) Schematic illustration of PSHE induced by an off-axis polarization singularity at the focal plane; the blue and red ellipses represent the separated left- (LCP) and right-handed circularly polarized (RCP) components, respectively.

where E_0 represents the amplitude; w_0 depicts the initial waist radius; m denotes the topological charges of the vortex phases of spin components; $\theta = 2 \arctan[(y_{in} + y_0)/(x_{in} + x_0)]$ is the angular coordinate of off-axis polarization singularity, and $(-x_0, -y_0)$ indicate the embedded position of polarization singularity, which is shown by a red dot in Fig. 1(a); θ_0 is a constant phase; $\{\mathbf{e}_L, \mathbf{e}_R\}$ are LCP and RCP basis vectors. To facilitate analysis, we translate the coordinate system to a new one (x, y) where polarization singularity is the coordinate origin, as shown in Fig. 1(b); then the center of the Gauss beam is located at (x_0, y_0) . By setting $x_0 = \delta \cos \alpha$, $y_0 = \delta \sin \alpha$, the two spin components $E_{R,L}(\rho, \varphi)$ of Eq. (1) in polar coordinates (ρ, φ) can be rewritten as

$$E_{R,L}(\rho, \varphi) = E_0 \exp\left(-\frac{\rho^2 + \delta^2}{w_0^2}\right) \exp\left(\frac{2\rho\delta \cos(\varphi - \alpha)}{w_0^2}\right) \times \exp[\pm im(\varphi + \varphi_0)]. \quad (2)$$

We set the amplitude part in Eq. (2) as $A(\rho, \varphi)$, which can be expanded into a series of OAM spectra with vortex phase $\exp(in\varphi)$ [41–43] as

$$A(\rho, \varphi) = E_0 \exp\left(-\frac{\rho^2 + \delta^2}{w_0^2}\right) \exp\left(\frac{2\rho\delta \cos(\varphi - \alpha)}{w_0^2}\right) = \sum_{n=-\infty}^{\infty} c_n(\rho) \exp(in\varphi), \quad (3)$$

where spectrum c_n is obtained by the angular Fourier transform:

$$c_n(\rho) = \frac{1}{2\pi} \int_0^{2\pi} A(\rho, \varphi) \exp(-in\varphi) d\varphi. \quad (4)$$

Then two spin components in Eq. (2) can be written as

$$E_{R,L}(\rho, \varphi) = E_0 \exp\left(-\frac{\rho^2 + \delta^2}{w_0^2}\right) \exp[\pm im(\varphi + \varphi_0)] \times \sum_{n=-\infty}^{\infty} I_n\left(\frac{2\rho\delta}{w_0^2}\right) \exp[in(\varphi - \alpha)], \quad (5)$$

where I_n is the modified Bessel function of the first kind [44] with integer order n . Therefore, it is clear that the off-axis vector Gauss beam can be viewed as the coherent superposition of a series of Bessel-Gauss (BG) beams with an on-axis topological charge $l_{R,L} = n \pm m$, i.e., $(n \pm m)\hbar$ OAM per photon.

The constant phase φ_0 in polar coordinates (ρ, φ) does not affect the OAM spectra, so we set $\varphi_0 = 0$. Due to the rotational symmetry of the Gauss beam concerning the coordinate origin, we also set $\alpha = 0$, and l th-order OAM spectra in spin components as $u_l(\rho, \varphi)$, with $u_l(\rho, \varphi) = E_0 \exp[-(\rho^2 + \delta^2)/w_0^2] I_n(2\rho\delta/w_0^2) \exp(il\varphi)$ depicting separable functions in polar coordinates, i.e., $u_l(\rho, \varphi) = R(\rho)F(\varphi)$; then $R(\rho) = E_0 \exp[-(\rho^2 + \delta^2)/w_0^2] I_n(2\rho\delta/w_0^2)$ and $F(\varphi) = \exp(il\varphi)$. The Fourier transform of $u_l(\rho, \varphi)$ is given by

$$\mathcal{F}[u_l(\rho, \varphi)] = (-i)^l \exp[il\phi] \mathcal{H}_l[R(\rho)] = \exp[il\phi - i\pi/2] \mathcal{H}_l[R(\rho)], \quad (6)$$

where (r, ϕ) are polar coordinates at the Fourier transform plane, and $\mathcal{H}_l[R(\rho)]$ represents an l th-order Hankel transform [45] of the radially symmetric function $R(\rho)$. Equations (5) and (6) imply that OAM spectra of two spin components have the same amplitude with opposite vortex phases and additional phases when $l_L = -l_R$, owing to $I_n(2\rho\delta/w_0^2) = I_{-n}(2\rho\delta/w_0^2)$ and $(-1)^l \mathcal{H}_l[R(\rho)] = \mathcal{H}_{-l}[R(\rho)]$. These OAM spectra in LCP and RCP components are in one-to-one correspondence, so the two spin components have a phase difference π at the focal plane. The maximum intensity positions of two spin components are origin symmetric, which means that the spin-dependent separation could be induced by the off-axis polarization singularity and observed at the focal planes of the thin lens.

Figure 1(c) schematically shows the focusing dynamic of the Gauss beam embedded with an off-axis polarization singularity located at $(0.4w_0, 0)$ in Cartesian coordinates (x_{in}, y_{in}) ; it can be seen that the propagating beam splits into two independent spin components along the y_f direction at the focal plane. Note that the spin-dependent separated distance, the separating direction, and the OAM spectra are closely related to the embedded position and polarization order of polarization singularity from Eqs. (5) and (6); the subsequent simulations and experiments will elucidate the corresponding relationships in detail.

To clarify the weight coefficient of each OAM state, we set $P(n)$ as the OAM power spectrum, which means the probability of a photon with $n\hbar$ OAM could be obtained by integrating $|c_n|^2$ along the radial direction,

$$S = \sum_{n=-\infty}^{\infty} \int_0^{\infty} |c_n(\rho)|^2 \rho d\rho, \quad (7)$$

$$P(n) = \frac{1}{S} \int_0^{\infty} |c_n(\rho)|^2 \rho d\rho,$$

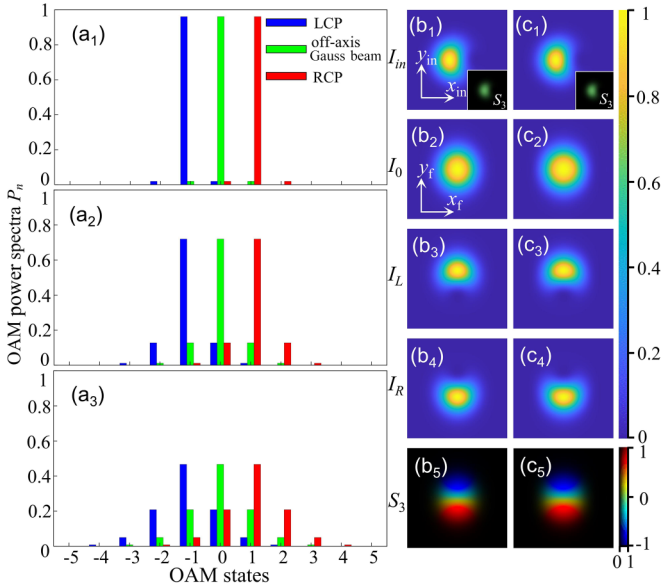


FIG. 2. OAM spectra of Gauss beam embedded with off-axis polarization singularity. (a₁)–(a₃) Normalized OAM power spectra $P(n)$ with $x_0 = -0.2w_0, -0.6w_0, -w_0$, and $y_0 = 0$; the blue, red, and green bars represent LCP and RCP components of off-axis vector Gauss beam ($m = 1$) and off-axis scalar Gauss beam, respectively. (b₁)–(b₅), (c₁)–(c₅) Comparison of off-axis vector Gauss beam and light field constructed from the superposition of OAM spectra in the case of $x_0 = -w_0, y_0 = 0$, and $m = 1$. From top to bottom: initial field intensities, focal field intensities, LCP intensities, RCP intensities, and S_3 distributions in focal field. Insets: S_3 distributions of initial fields.

where S is the beam power at the transverse plane. First, we explore the influences of the embedded position $(-x_0, -y_0)$ on the OAM spectra; Figures 2(a₁)–2(a₃) show the normalized power spectra $P(n)$ of two spin components of the off-axis vector Gauss beam ($m = 1$) when $x_0 = -0.2w_0, -0.6w_0, -w_0$, and $y_0 = 0$. As shown in Figs. 2(a₁)–2(a₃), the OAM spectra [blue (red) bars] of the left- (right-) handed circularly polarized component moves to the left (right) by one unit compared to the situation of off-axis scalar Gauss beams (green bars) without the vortex phase. The power of the OAM spectra ($|n \pm m| \neq 1$) increases with the increased off-axis displacement δ .

The dispersion of the OAM power spectrum has a relationship with the displacement δ in the form $[\sum_{-\infty}^{\infty} n^2 P(n)]^{1/2} = \delta/w_0$, with n denoting the order of the OAM spectrum. In addition, the power of OAM spectra with the topological charge $|n \pm m| > 3$ is negligible in the two spin components, respectively. We compare the simulation results of an off-axis vector Gauss beam with a light field constructed from the superposition of seven OAM spectra with $|n \pm m| \leq 3$. Figures 2(b₁)–2(b₅) and 2(c₁)–2(c₅), from top to bottom, display initial field intensities, focal field intensities, LCP intensities, RCP intensities, and S_3 distributions (drawn with total intensity as background) in the focal field, respectively. We set the parameters $\lambda = 632.8$ nm, $w_0 = 1.089$ mm, $x_0 = -w_0, y_0 = 0, m = 1$, and $f = 20$ cm. It can be seen that the rotational symmetry of the initial intensity distribution with $S_3 = 0$ is

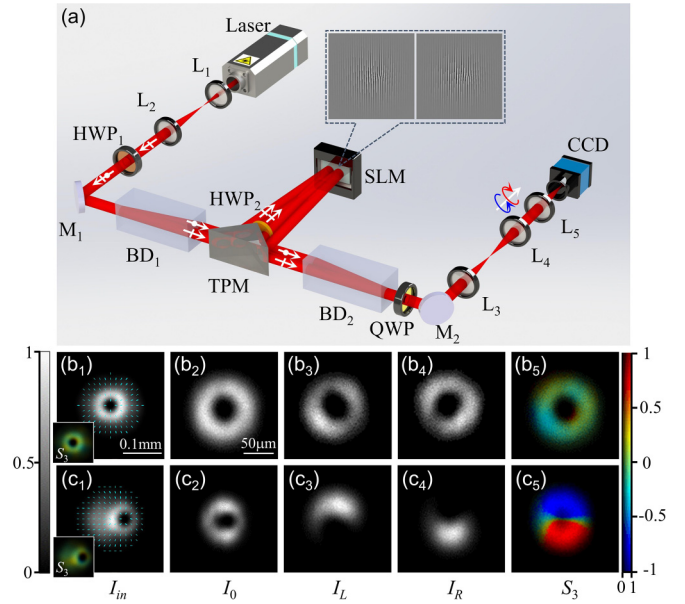


FIG. 3. Experimental observation of PSHE with off-axis polarization singularity. (a) Experimental setup for generating off-axis vector Gauss beam (the arrows with white short lines and dots represent p - and s -polarized components, respectively). L_{1-5} , lenses; $M_{1,2}$, mirrors; $HWP_{1,2}$, half-wave plates; $BD_{1,2}$, beam deflector; TPM, triangle prism mirror (96° obtuse angles); SLM, spatial light modulator; QWP, quarter-wave plates; CCD, charge-coupled device. Insets, an example of CGH on the SLM; (b₁)–(b₅), (c₁)–(c₅) Experimentally measured initial total intensities with $x_0 = 0$ and $-0.4w_0, y_0 = 0, m = 1$. From left to right: initial field intensities (cyan lines represent states of polarization), focal field intensities, LCP intensities, RCP intensities, and S_3 distributions in focal field. Insets: S_3 distributions of initial fields.

broken from Fig. 2(b₁) and its inset; the corresponding total intensity distributions calculated by the Fresnel diffraction integral are elliptical at focal fields from Fig. 2(b₂); and two spin components have the same intensity distributions, but are symmetric about the x axis, as shown in Figs. 2(b₃) and 2(b₄). The centroids of the two spin components have a significant separation from Fig. 2(b₅). The corresponding superposed fields of multiple OAM spectra restore the focal results with high accuracy without noticeable differences, as shown in Figs. 2(c₁)–2(c₅). Therefore, the distribution and broadening of the OAM spectra can be manipulated by the topological charges m and the off-axis displacement δ ; then the increasing weight coefficients of the higher-order OAM spectra with larger dark core sizes will enhance the PSHE.

III. RESULTS AND DISCUSSIONS

To explore the influence of the above parameters on PSHE induced by off-axis polarization singularity, we experimentally studied the focusing dynamic of the off-axis vector Gauss beam. The experimental setup is shown in Fig. 3(a). A p -polarized Gaussian beam from a He-Ne laser (wavelength $\lambda = 632.8$ nm) is expanded and collimated by a lens set (L_1 and L_2); then it is converted into 45° linearly polarized light by a half-wave plate (HWP_1 with its fast axis oriented 22.5°

concerning the x axis) and through the first beam deflectors (BD_1) to get two parallel propagating beams with orthogonal polarization. Then the two decomposed light beams with linear polarizations (i.e., p - and s -polarized components) are modulated by two-dimensional computer-generated holograms [46] [CGHs, as shown in the inset of Fig. 3(a)] displayed on the spatial light modulator (SLM), respectively. Then they pass the second inverted beam deflectors (BD_2) for combination, both of them are converted into LCP and RCP constituents by a quarter-wave plate (QWP), and the first diffracting order is filtered and imaged at the back focal plane of a $4f$ filter system (L_3 and L_4); the focal field was recorded by the charge-coupled device (CCD) at the focal plane of the lens (L_5). The HWP₂ (fast axis oriented 45°) converts the s -polarized component into p -polarized light to be modulated by the SLM. We use the CGHs displayed on the SLM to precisely manipulate the embedded position and the topological charge of the off-axis polarization singularity [47].

Figures 3(b₁)–3(b₅) and 3(c₁)–3(c₅) show the measurement results of the Gauss beam with on-axis and off-axis first-order polarization singularity. Panels from left to right are the initial total intensity (I_{in}) and Stokes parameters S_3 (insets), focal field intensity (I_0), two spin components (I_L and I_R), and Stokes parameters S_3 at the focal plane, respectively. In experiment, all parameters are selected as $\lambda = 632.8$ nm, $w_0 = 1.089$ mm, $x_0 = 0$, $-0.4w_0$, $y_0 = 0$, $m = 1$, and $f = 20$ cm. Figures 3(b₁) and 3(b₂) show that the radially polarized Gauss beam with $S_3 = 0$ has a dark core at the center of the initial and focal plane, and two spin components have the same intensity distribution with the shape of donuts as shown in Figs. 3(b₃) and 3(b₄); Fig. 3(b₅) indicates that the focal spot is linearly polarized with $S_3 = 0$. It meets the expectation that the radial polarized Gauss beam maintains its polarization distribution when it is focused by the thin lens. When the polarization singularity deviates from the center along the x axis with a shift $x_0 = -0.4w_0$, the polarization distribution maintains radial polarization with $S_3 = 0$ around the shifted dark core at the initial plane, as shown in Fig. 3(c₁) and its inset. In contrast, the shifted circular dark core evolves into an elliptical dark core located at the center of the focal plane with the two spin constituents dominating the upper (I_L) and lower (I_R) parts, respectively, evidenced by the measured intensity distributions in Figs. 3(c₃) and 3(c₄). This is further confirmed by the Stokes parameter S_3 distribution in Fig. 3(c₅), which represents the giant PSHE.

Next, we demonstrate that the proposed controllable PSHE induced by off-axis polarization singularity can be pre-designed along the arbitrary direction, which may bring extra advantages for PSHE-based imaging techniques such as edge imaging [48,49]. Figure 4 gives two examples of PSHE along the y and x directions by presetting polarization singularity shifted along the x and y directions, respectively. The designed polarization singularity is illustrated in the left column of Fig. 4. When the polarization singularity is located at $(-0.4w_0, 0)$ as shown in Figs. 4(a₁)–4(a₅) show that the two spin components are the upper (I_R) and lower (I_L) parts of the total intensity distribution, respectively. Their separated direction is opposite to the situation as shown in Fig. 3(c₅), where the polarization singularity is shifted along the positive x direction. In contrast, when the polarization singularity is

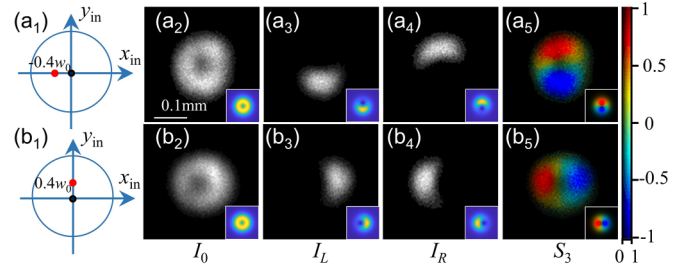


FIG. 4. Controllable PSHE along designed directions. (a₁), (b₁) Embedded position of polarization singularity with $(-0.4w_0, 0)$ and $(0, 0.4w_0)$. (a₂)–(a₅), (b₂)–(b₅) Experimentally measured total intensity distributions (I_0), two spin components (I_L and I_R), and Stokes parameters S_3 at the focal plane. Insets: simulated results.

located at $(0, 0.4w_0)$ as shown in Figs. 4(b₁)–4(b₅) show that the two spin components are the left (I_R) and right (I_L) parts of the total intensity distribution. It is clear that the spin splitting direction can be determined by manipulating the position of the polarization singularity at the initial parameter setting stage, which provides an extra knob to manipulate the PSHE compared to previously reported PSHE of vector beams [34,35,50]. Therefore, we conclude that the spin-dependent separating direction is perpendicular to the off-axis direction of polarization singularity.

Finally, we demonstrate the controllable separated distances of PSHE by manipulating the off-axis displacement

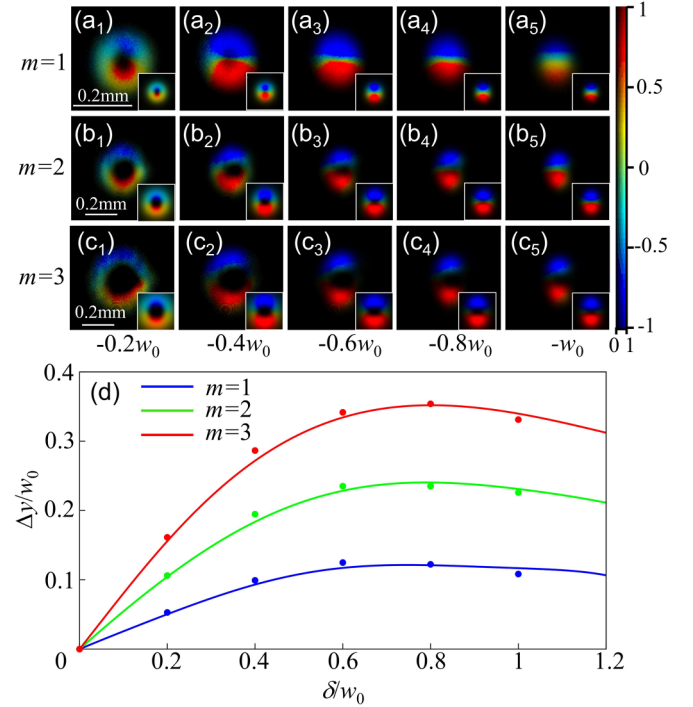


FIG. 5. The controllable separated distances of PSHE. (a)–(c) Experimentally measured Stokes parameters S_3 at focal plane with different embedded positions when $m = 1, 2$, and 3 . Insets: simulated results. (d) The trends of separated distances with the increase of off-axis displacement; blue, green, and red lines represent the simulated results with $m = 1, 2, 3$, and the dots with corresponding color represent the measured results, respectively.

and polarization order of the polarization singularity. Figure 5 shows the experimental results at the focal planes with $m = 1, 2, 3$, $x_0 = -0.2w_0, -0.4w_0, -0.6w_0, -0.8w_0, -w_0$, and $y_0 = 0$. It displays the measured Stokes parameters (top three rows) and the changing trends of the spin-dependent separated distance of two spin components, respectively. The separated distances Δy get larger with the increase of polarization order of polarization singularity at the focal center, and the sizes of the focal spot get smaller with increasing off-axis displacement δ . The OAM spectra mainly present the m th-order OAM component with other components of tiny power when the off-axis displacement is minor, as shown in Fig. 2(a₁). For this reason, the off-axis vector beams present donut shapes, as shown in Fig. 5(a₁). The power of other components increases with increased off-axis displacement, and the $(m \pm 1)$ -th-order OAM components increase significantly, as shown in Figs. 2(a₂) and 2(a₃), so the 0th-order OAM spectra components with larger power present a solid spot when $m \pm 1 = 0$, as shown in Figs. 5(a₃)–5(a₅). The separated distances Δy first increase and then decrease with the increasing of off-axis displacement, as shown in Fig. 5(d), and the maximum separation reaches $0.34w_0$ when $m = 3$ and $\delta = 0.8w_0$, as shown by the red line in Fig. 5(d). The increased m naturally enlarges the separated distances Δy at the focal plane, due to the larger dark core size of the higher vortex mode. Note that the maximum power weight of higher-order OAM spectra is limited owing to the limited Gauss beam waist (i.e., $\delta \leq w_0$), which leads to a maximum separated distance Δy when $\delta = 0.8w_0$.

IV. CONCLUSIONS

In conclusion, the controllable PSHE at focal planes of the Gauss beam with an initial polarization singularity shifted from its center is represented, and the results show that the spin-dependent separating direction is always perpendicular to the off-axis direction of polarization singularity. The embedded position and polarization order of polarization singularity could significantly influence the spin-dependent separated distance and the OAM spectrum of vector Gauss beams. The separated spin distances increase with the polarization order of polarization singularity when the off-axis displacement is fixed; in contrast, the separated spin distances increase first with off-axis displacement and then decrease. The connection between PSHE and the broadening of the OAM spectrum is revealed. We believe the reported PSHE induced by off-axis polarization singularity could contribute to the SOI and manufacturing of optical spin filters.

ACKNOWLEDGMENTS

This research was supported by the National Key Research and Development Program of China (Grant No. 2022YFA1404800); the National Natural Science Foundation of China (NSFC) (Grants No. 12174309, No. 12074312, No. 12074313, and No. 62305271); the Fundamental Research Funds for the Central Universities (Grant No. 5000230111); and the Shaanxi Fundamental Science Research Project for Mathematics and Physics (Grant No. 22JSY013).

-
- [1] S. Liu, S. Chen, S. Wen, and H. Luo, *Opto-Electron. Sci.* **1**, 220007 (2022).
 - [2] X. Ling, X. Zhou, K. Huang, Y. Liu, C.-W. Qiu, H. Luo, and S. Wen, *Rep. Prog. Phys.* **80**, 066401 (2017).
 - [3] X. Zhou, Z. Xiao, H. Luo, and S. Wen, *Phys. Rev. A* **85**, 043809 (2012).
 - [4] X. Zhou, X. Ling, H. Luo, and S. Wen, *Appl. Phys. Lett.* **101**, 251602 (2012).
 - [5] Y. Zhao, J. S. Edgar, G. D. M. Jeffries, D. McGloin, and D. T. Chiu, *Phys. Rev. Lett.* **99**, 073901 (2007).
 - [6] H. Adachi, S. Akahoshi, and K. Miyakawa, *Phys. Rev. A* **75**, 063409 (2007).
 - [7] T. Zhu, Y. Lou, Y. Zhou, J. Zhang, J. Huang, Y. Li, H. Luo, S. Wen, S. Zhu, Q. Gong, M. Qiu, and Z. Ruan, *Phys. Rev. Appl.* **11**, 034043 (2019).
 - [8] J. Zhou, H. Qian, C.-F. Chen, J. Zhao, G. Li, Q. Wu, H. Luo, S. Wen, and Z. Liu, *Proc. Natl. Acad. Sci. USA* **116**, 11137 (2019).
 - [9] J. Sinova, S. O. Valenzuela, J. Wunderlich, C. H. Back, and T. Jungwirth, *Rev. Mod. Phys.* **87**, 1213 (2015).
 - [10] M. Onoda, S. Murakami, and N. Nagaosa, *Phys. Rev. Lett.* **93**, 083901 (2004).
 - [11] S. Franke-Arnold, L. Allen, and M. Padgett, *Laser Photonics Rev.* **2**, 299 (2008).
 - [12] K. Y. Bliokh, A. Niv, V. Kleiner, and E. Hasman, *Nat. Photonics* **2**, 748 (2008).
 - [13] O. Hosten and P. Kwiat, *Science* **319**, 787 (2008).
 - [14] K. Y. Bliokh, F. J. Rodríguez-Fortuño, F. Nori, and A. V. Zayats, *Nat. Photonics* **9**, 796 (2015).
 - [15] Y. Zhang, P. Li, S. Liu, L. Han, H. Cheng, and J. Zhao, *Appl. Phys. B* **122**, 184 (2016).
 - [16] L. Marrucci, C. Manzo, and D. Paparo, *Phys. Rev. Lett.* **96**, 163905 (2006).
 - [17] H. Li, C. Ma, J. Wang, M. Tang, and X. Li, *Opt. Express* **29**, 39419 (2021).
 - [18] S. Liu, S. Qi, Y. Li, B. Wei, P. Li, and J. Zhao, *Light Sci. Appl.* **11**, 219 (2022).
 - [19] Y. Li, Y. Zou, S. Liu, P. Li, B. Wei, and J. Zhao, *Photonics Res.* **11**, 1553 (2023).
 - [20] K. Y. Bliokh, C. T. Samlan, C. Prajapati, G. Puentes, N. K. Viswanathan, and F. Nori, *Optica* **3**, 1039 (2016).
 - [21] K. Y. Bliokh, C. Prajapati, C. T. Samlan, N. K. Viswanathan, and F. Nori, *Opt. Lett.* **44**, 4781 (2019).
 - [22] A. V. Nalitov, G. Malpuech, H. Terças, and D. D. Solnyshkov, *Phys. Rev. Lett.* **114**, 026803 (2015).
 - [23] K. Y. Bliokh, Y. Gorodetski, V. Kleiner, and E. Hasman, *Phys. Rev. Lett.* **101**, 030404 (2008).
 - [24] Y. Liu, Y. Ke, H. Luo, and S. Wen, *Nanophotonics* **6**, 51 (2017).
 - [25] Z. Xie, T. Lei, H. Qiu, Z. Zhang, H. Wang, and X. Yuan, *Photonics Res.* **8**, 121 (2020).
 - [26] Z. Liu, Y. Liu, Y. Ke, Y. Liu, W. Shu, H. Luo, and S. Wen, *Photonics Res.* **5**, 15 (2017).
 - [27] P. Li, S. Liu, and J. Zhao, *Prog. Opt.* **68**, 191 (2023).

- [28] T. Zhao, S. Zhang, Y. Guo, and Q. Wang, *Nanoscale* **8**, 233 (2016).
- [29] Y. Tsuru, Y. Kozawa, Y. Uesugi, and S. Sato, *Opt. Lett.* **49**, 1405 (2024).
- [30] X. L. Wang, J. Chen, Y. Li, J. Ding, C. S. Guo, and H. T. Wang, *Phys. Rev. Lett.* **105**, 253602 (2010).
- [31] X. Xie, Y. Chen, K. Yang, and J. Zhou, *Phys. Rev. Lett.* **113**, 263901 (2014).
- [32] V. Parigi, V. D'Ambrosio, C. Arnold, L. Marrucci, F. Sciarrino, and J. Laurat, *Nat. Commun.* **6**, 7706 (2015).
- [33] X. Ouyang, Y. Xu, M. Xian, Z. Feng, L. Zhu, Y. Cao, S. Lan, B.-O. Guan, C.-W. Qiu, M. Gu, and X. Li, *Nat. Photonics* **15**, 901 (2021).
- [34] Y. Liu, X. Ling, X. Yi, X. Zhou, S. Chen, Y. Ke, H. Luo, and S. Wen, *Opt. Lett.* **40**, 756 (2015).
- [35] Y. Zhang, P. Li, S. Liu, and J. Zhao, *Opt. Lett.* **40**, 4444 (2015).
- [36] X. Ling, F. Guan, X. Cai, S. Ma, H. Xu, Q. He, S. Xiao, and L. Zhou, *Laser Photonics Rev.* **15**, 2000492 (2021).
- [37] J. Wang, L. Shi, and J. Zi, *Phys. Rev. Lett.* **129**, 236101 (2022).
- [38] M. Mazanov, O. Yermakov, A. Bogdanov, and A. Lavrinenko, *APL Photonics* **7**, 101301 (2022).
- [39] W. Zhu, H. Zheng, Y. Zhong, J. Yu, and Z. Chen, *Phys. Rev. Lett.* **126**, 083901 (2021).
- [40] Y. Li, Z. Zhu, X. Wang, L. Gong, M. Wang, and S. Nie, *J. Opt. Soc. Am. A* **31**, 2356 (2014).
- [41] M. V. Vasnetsov, V. A. Pas'ko, and M. S. Soskin, *New J. Phys.* **7**, 46 (2005).
- [42] A. M. Yao and M. J. Padgett, *Adv. Opt. Photonics* **3**, 161 (2011).
- [43] A. D'Errico, R. D'Amelio, B. Piccirillo, F. Cardano, and L. Marrucci, *Optica* **4**, 1350 (2017).
- [44] S. R. Seshadri, *J. Opt. Soc. Am. A* **24**, 2837 (2007).
- [45] M. Guizar-Sicairos and J. C. Gutiérrez-Vega, *J. Opt. Soc. Am. A* **21**, 53 (2004).
- [46] Y. Zhang, P. Li, C. Ma, S. Liu, H. Cheng, L. Han, and J. Zhao, *Appl. Opt.* **56**, 4956 (2017).
- [47] S. Liu, S. Qi, Y. Zhang, P. Li, D. Wu, L. Han, and J. Zhao, *Photonics Res.* **6**, 228 (2018).
- [48] J. Zhang, S. Zhou, X. Dai, M. Huang, and X. Yu, *Opt. Express* **31**, 6062 (2023).
- [49] S. He, Y. Shou, D. Xu, Q. Yang, J. Liu, S. Chen, and H. Luo, *Phys. Rev. Appl.* **21**, 034045 (2024).
- [50] X. Ling, X. Yi, X. Zhou, Y. Liu, W. Shu, H. Luo, and S. Wen, *Appl. Phys. Lett.* **105**, 151101 (2014).